

Final Report for TWDB Contract No. 1004831127

Sediment Transport Modeling of Channel Scale Geomorphic Processes

J.K. Haschenburger
University of Texas at San Antonio

July 31, 2012

2012 AUG 17 AM 8:24

CONTRACT ADMINISTRATION

Final Report for TWDB Contract No. 1004831127

Sediment Transport Modeling of Channel Scale Geomorphic Processes

J.K. Haschenburger
University of Texas at San Antonio

July 31, 2012

1 Introduction

This study investigated the use of a two-dimensional (2D) modeling strategy to predict channel adjustment in the lower San Antonio River in response to a range of flood magnitudes. The modeling strategy was employed in one study reach near Goliad and validated with empirical observations where possible. The 2D model permits a more detailed examination of the morphological response of the streambed compared to a one-dimensional (1D) model.

This report is divided into six sections. Section 2 briefly describes the study reach, while section 3 explains the data collection and analysis of field observations used in model development and validation. A brief overview of the selected model River2D-Morphology (R2DM) is described in section 4 along with the specific model setup for the Goliad study reach. Section 5 contains the analysis of the simulated flood events, which is followed by concluding comments.

2 Study reach

A previous investigation (Haschenburger and Curran, 2012) used three channel reaches, identified as Floresville, Charco, and Goliad, to model streambed adjustment using the 1D HEC-RAS model. This study focuses on the Goliad reach (Figure 1, Table 1) and utilizes a portion of the reach, which is about 3 km (1.9 mi) long, because detailed information about the bed topography is available. Bed topography information is critical input data for higher dimensional modeling.

Table 1. Characteristics of the Goliad study reach used in HEC-RAS modeling¹

Length	Mean bankfull width	Mean bankfull depth	Bed morphology	Large woody debris
4.2 km (2.6 mi)	47.2 ± 8 m (154.9 ± 2.7 ft)	5.0 ± 0.3 m (16.7 ± 1.1 ft)	Presence of channel bars	Minor presence; mostly along channel margins

¹ Error bars are standard errors

3 Empirical database for model development and validation

3.1 Channel boundary characteristics

3.1.1 Channel configuration

A three-dimensional depiction of the study reach topography was created by collecting bathymetry data from the wetted channel and combining them with land survey of exposed portions of the bed and existing LiDAR observations of the banks and floodplain. Data collection and processing were completed by the Texas Water Development Board and their affiliates.

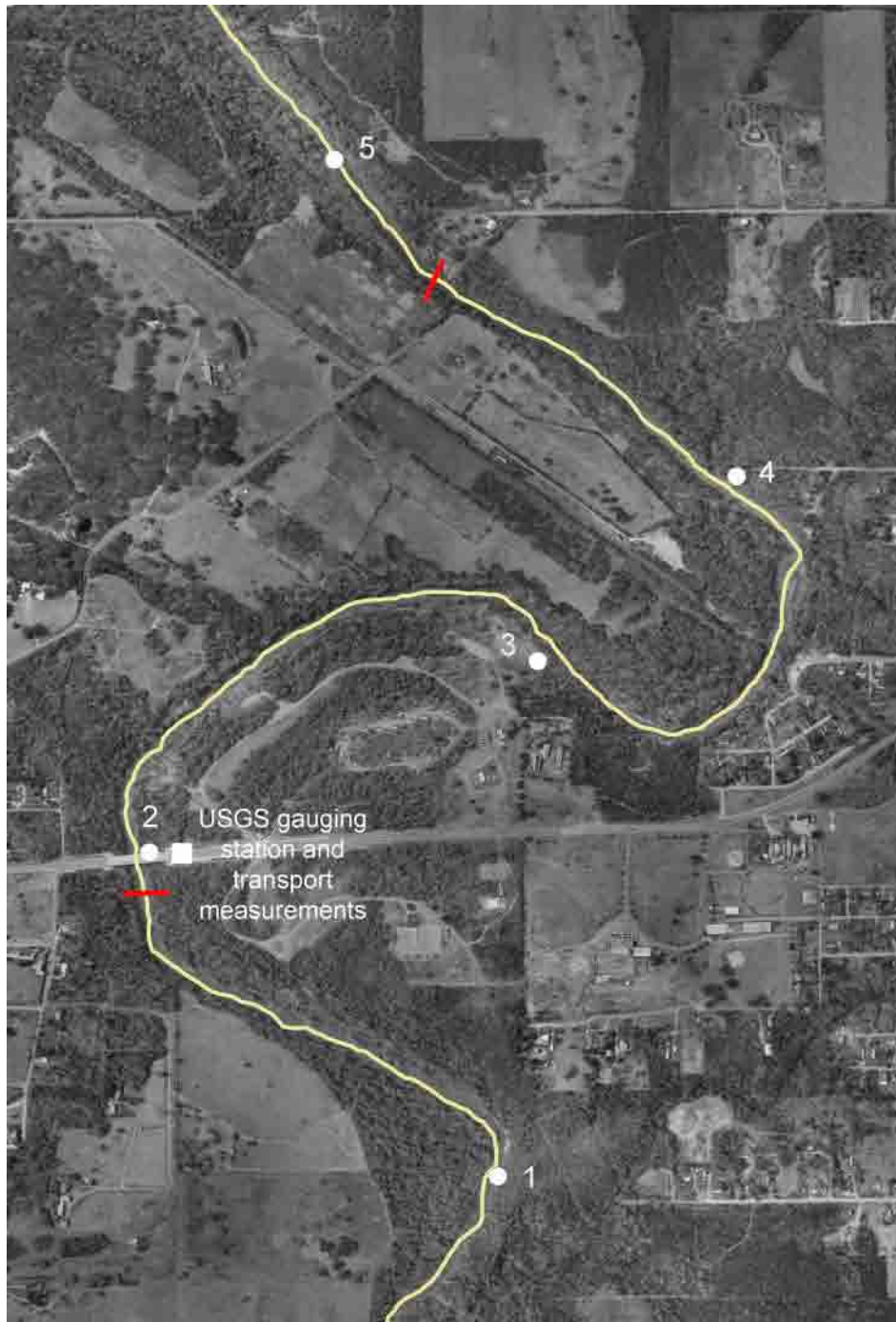


Figure 1. The Goliad reach. Locations of channel cross-sectional survey and boundary material sampling shown by circles. Location of US Geological Survey (USGS) streamflow gauging and sediment transport measurements shown by square. The limits to the study reach used in this study are indicated by red lines.

3.1.2 Boundary materials

Sediment samples were collected along each of the surveyed cross sections. All samples were collected by a grab technique and therefore represent near surface sediments. In general, characteristics of sediments are based on between 4 to 10 samples of streambed sediments depending on channel bed width, 6 samples of bank sediments (3 per bank), and 6 samples of floodplain sediments where possible (3 per surface).

All sediments were wet sieved to remove fines (0.063 mm; <0.0025 in.). The remaining coarser sediments were dry sieved. Grain size fractions were characterized by 0.5 phi increments. The size distribution for a given depositional environment was calculated as a weighted mean to represent the boundary materials of the cross section.

Boundary materials are dominated by sand sized sediments (Table 2). Bed sediment contains a significant portion of sand (~85%). Bank materials are mostly sand with a high percent of silt and clay. Floodplain sediment contains 49% silt-clay and 51% sand. Associated bulk porosities were estimated based on the median grain size diameter using Komura's (1961) equation for river sediment, while the angle of repose was derived from available information.

Table 2. Boundary materials by grain size categories¹

Environment	% Silt-clay	% Sand	% Gravel
Bed	8.2	85.3	6.5
Bank	40.8	59.0	0.2
Floodplain	48.9	50.9	0.2

¹ Silt-Clay: Diameter (D) <0.063 mm (0.0025 in.);
Sand: <0.063 mm (0.0025 in.) ≤ D < 2 mm (0.079 in.);
Gravel: D ≥ 2 mm (0.079 in.)

3.2 Flow and sediment transport

3.2.1 Flood events

Streamflow records of stage and discharge magnitude are available at the Goliad gauging station (08188500) operated by the US Geological Survey (USGS) (Figure 1). Mean daily flows were used in a flow duration analysis, while the instantaneous record (i.e., 15 minute series) provided the basis for flood hydrographs.

3.2.2 Bedload transport rates

Bedload observations were collected by deploying a 7.6 cm (3 inch) orifice Helley-Smith bedload sampler with a 0.20 mm (0.0079 in.) mesh collection bag from the gauging bridge (Figure 1). The orifice size was sufficiently large relative to the largest grain sizes present locally on the streambed to permit capture of all potentially mobile grain sizes.

Collection proceeded using a fixed width interval strategy along the cross section aiming for 20 samples. Nonetheless, early in the sampling program, one 10 sample effort was completed to

ensure at least some observations given the unpredictability of floods. For each sample, the Helley-Smith sampler rested on the bed for 1 to 10 minutes, depending on the flow conditions. Bedload samples were wet sieved to remove suspended sediment collected while the sampler was submerged. Sediment larger than 0.063 mm (≥ 0.0025 in.) was dry sieved into 0.5 phi size increments. Only sediment larger than the size of the mesh of the collection bag is considered in bedload rates. Cross-sectional rates were computed by summing the individual bedload transport rates applied over their respective width increments.

Bedload transport rates are relatively low and range from 0.012 kg s⁻¹ (0.026 lb s⁻¹) to 2.0 kg s⁻¹ (4.4 lb s⁻¹) for flow rates corresponding to 3.6 m³s⁻¹ (129 ft³s⁻¹) and 265 m³s⁻¹ (9360 ft³s⁻¹), respectively. These flow rates have exceedence probabilities of 1 to 81%, respectively, with the largest observed flow slightly exceeding bankfull capacity. A rating curve was fitted using least squares regression (Figure 2) and then used to estimate total bedload flux for selected flood hydrographs.

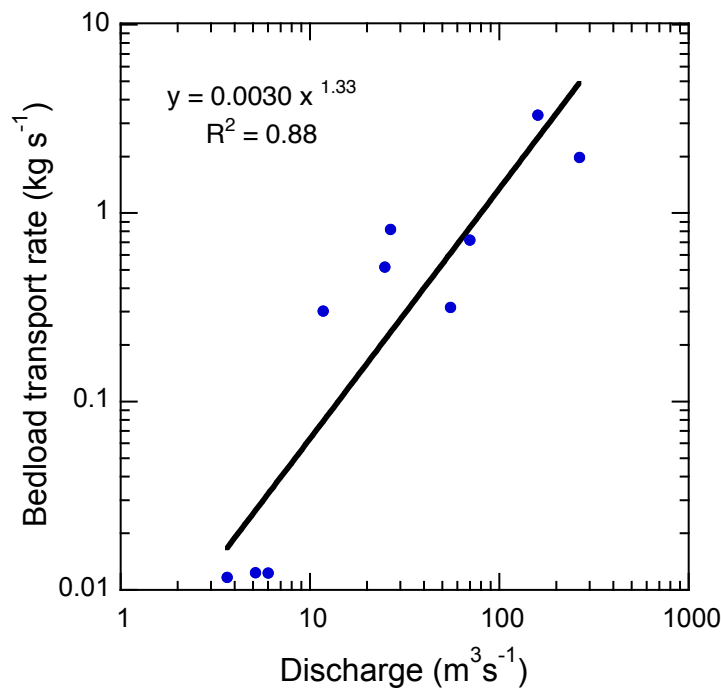


Figure 2. Bedload transport rates as a function of flow discharge for the Goliad sampling site.

3.2.3 Change in bed elevation

Documentation of change in streambed elevation in response to floods is limited to one estimate for cross sections 2-4 (Figure 1). Observations of the change in bed elevation were derived by comparing the cross-sectional survey of cross sections 2, 3, and 4 with information extracted from a raster depiction of bed topography produced by another Texas Water Development Board project. The cross sections were surveyed to capture major breaks in slope. Latitude and longitude coordinates were established by collecting and differentially correcting a benchmarked observation using a GPS unit. Where land access was not possible, survey of the flow channel was extended to the floodplain using available LiDAR coverage. For the raster format, cross-

sectional information could not be extracted exactly at the surveyed cross sections, given the software that was available for cross-sectional extraction. Nonetheless, they are in close proximity. At each location cross sections were overlaid and the net change in bed area computed, ignoring changes in bank erosion or deposition. This comparison provides an order of magnitude metric from which to assess general model performance.

4 2D modeling

4.1 Model selection and justification

R2DM is an open source extension of River2D (R2D) with the capability to model mobile streambeds and therefore changes in bed morphology caused by floods. The open source R2D model is a depth averaged hydrodynamic model with capabilities to model steady and unsteady flow and specific modules to model aspects of fish habitat and river ice processes. This project utilized R2DM because it is a well-respected, open source 2D model that has been applied globally and a key developer, Dr. Stephen Kwan, continues to work on the model. Further, previous work for the Texas Instream Flow Program has taken advantage of the habitat capability of R2D. Its overall capacity for modeling both biological conditions and geomorphological adjustments at different flow rates simplifies the process when both aspects are of interest. Only one setup is needed to establish channel boundary conditions, which results in significant gains in time and cost efficiency when assessing prescribed instream flows.

4.2 Model description

The hydrodynamics of River2D are based on the 2D vertically averaged St. Venant equations (Steffler and Blackburn, 2002). The model solves the equations for conservation of water mass and two components of the momentum vector to derive water depth and discharge intensities in the streamwise and crosswise directions. Key assumptions include a hydrostatic pressure distribution in the vertical, constant distributions of horizontal velocities over depth, and negligible effects from Coriolis and wind forces.

Specific development of the R2D model assumes bed shear stresses are related to the magnitude and direction of the depth-averaged velocity and set the friction slope. The distribution of roughness is based on an effective roughness height because this parameter tends to remain constant over a wider range of flow depths than Manning's n . Initial values are finalized by calibrating the model to known water surface elevations and flow velocities. A Boussinesq type eddy viscosity approach partitions an eddy viscosity coefficient into three parts to compute transverse turbulent shear stresses. The transition from wet and dry areas during unsteady flow is handled through a strategy of changing surface flow equations to groundwater flow equations to derive a continuous free surface. A Finite Element Method based on the streamline upwind Petrov-Galerkin weighted residual formulation is used. Equations can be solved directly or iteratively using the Newton Raphson method.

The R2DM morphodynamics extension of R2D to model mobile beds determines streambed adjustment by solving the Exner equation for sediment continuity (Vasquez and Kwan, 2009). The transport conditions are set by entering sediment property variables (e.g., porosity) and

assigning values to numerous parameters that describe sediment transport conditions. There is a capacity to model the degree to which sediment transport is diffusive or convective by setting a sediment upwinding factor, the latter being important when bedforms are present. R2DM employs a simple first order up-winding method where sediment flux through each boundary of a given mesh cell is calculated by averaging results of local nodes. To adjust for the role that bed slope plays in driving the direction of bedload transport, a tranverse slope calibration factor is available. Finally, although the model is 2D, there is a semi-empirical correction for secondary flow circulation that is known to develop in meander bends. This correction assumes a spiral flow locally and is fixed for the modeled reach. A related inertial adaptation correction employed when selecting the secondary flow option is implemented through a calibration factor.

R2DM implements only bedload transport equations to predict rates of sediment transport. Any sediment that goes into suspension where velocity is sufficiently high is deposited downstream in lower velocity areas (Vasquez and Kwan, 2009). Five bedload transport equations are incorporated into R2DM so that different river types can be accommodated: (1) Meyer-Peter and Muller equation (1948), (2) Engelund-Hansen equation (1967), (3) Van Rijn equation (1984), Kassem and Chaudhry empirical equation (1998), and the (5) Wilcock-Crowe (2003) equation. Additional input parameters are needed with the last equation (e.g., specific bed material size distribution).

4.3 Model setup and input parameters

The general modeling procedure is to develop a computational mesh from channel topography information, calibrate the hydrodynamic model for a given flow rate by adjusting roughness values based on field observations, and then run a steady flow model that is the initial setup for an unsteady flow model. The addition of sediment properties and transport conditions and the definition of inflow and outflow boundary conditions complete the necessary steps for unsteady flow simulations of a mobile streambed.

4.3.1 Computational mesh

As part of another Texas Water Development Board project bed topography was converted to a computational mesh and calibrated with field observations for input into R2D as a .cdg file. The mesh size is about 2 m within the channel but larger for banks and floodplain areas of the study reach. The mesh quality index is 0.33, which meets the recommended quality for R2D. Only a subset of the executed steady flow models is used in this study (Table 3).

Table 3. Existing steady flow models used in this study

File name	Discharge, m ³ s ⁻¹
19036_2m_I_02p690.cdg	2.69
19036_2m_I_03p398.cdg	3.40
19036_2m_I_11p553.cdg	11.55

4.3.2 Flow parameters and boundary conditions

Table 4 outlines the flow parameters and boundary conditions in R2DM and the values used for the Goliad reach.

Table 4. Set up for flow parameters and conditions under Flow options and Edit flow boundary

Category	Variables, parameters, and input data	Default or typical values ¹	Goliad reach
Flow parameters	Eddy viscosity coefficient	$\epsilon_1 = 0$	$\epsilon_1 = 0$
		$\epsilon_2 = 0.5$	$\epsilon_2 = 0.5$
		$\epsilon_3 = 0.1$	$\epsilon_3 = 0.1$
	Upwinding coefficient for unsteady flow	0.25	0.25
	Minimum depth for groundwater flow (wet-dry transition)	0.01	0.01
	Groundwater transmissivity	0.1	0.1
	Groundwater storativity	1	0.25
Flow boundary conditions	Upstream boundary condition	3 options ²	15 minute flow rate series
	Downstream boundary condition	5 options ²	15 minute stage series

¹ see manual for typical values; default values appear in the parameter fields in R2DM

² see flow options in R2DM

For the upwinding coefficient, Hicks and Steffler (1992) suggested a value of 0.25 be used for unsteady flow simulations but a value of 0.5 for steady flow simulations. Sensitivity analysis of the groundwater storativity parameter indicated that changing the default value of 1 to 0.25 improved the match of the inflow and outflow hydrographs in the test run (Figure 3). For unsteady flow, the inflow boundary condition is the 15 minute series of discharge from the Goliad streamflow gauging station, while the outflow boundary condition is the associated stage referenced to a local elevational datum.

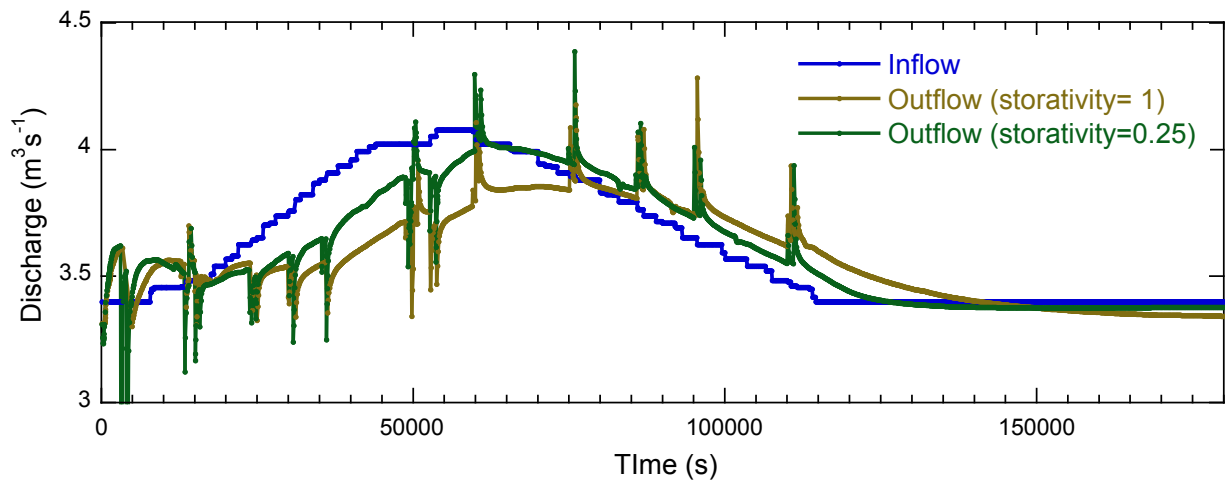


Figure 3. Comparison of outflow hydrographs modeled with different groundwater storativity values.

4.3.3 Sediment parameters and transport conditions

Sediment options include variables to describe bed material properties, select a transport function, define the nature of sediment movement through parameters, and set the degree to which the streambed can adjust (Table 5).

Table 5. Set up for sediment-related parameters and conditions under Sediment options

Category	Variables, parameters, and input data	Default or typical values ¹	Goliad reach
Sediment transport	Transport function	5 functions ²	Engelund-Hansen
	Transversal slope factor	1.5	1.25
	Upwinding factor	0.25	0.9
	Minimum flow depth for sediment transport (m)	0.001	0.07
Sediment properties	Median diameter (m)		0.00032
	Porosity (proportion)		0.42
	Angle of repose (%)		35
Streambed	Bed elevation boundary condition	4 options ³	Free
Sediment supply	Specific volumetric transport rate (m ² s ⁻¹)		Not activated
Flow correction	Secondary flow correction		Not activated
	Inertial adaptation length factor	0.4 to 2	Not activated

1 see manual for typical values; default values appear in R2DM

2 see section 4.2 and R2DM manual

3 see sediment options in R2DM

Based on the equation specifications and conditions of development, the Engelund-Hansen equation is the only viable option for the study reach. The equation was calibrated using flume data with grain sizes from 0.19 to 0.93 mm and therefore is applicable to sand-bed channels. Typically employed as a total load equation, Vasquez and Kwan (2009) implemented a bedload transport only function into R2DM, which is given as

$$q_s = \frac{0.05C^2}{g} \sqrt{g(s-1)D_{50}^3 \tau^{*1.5}}$$

where q_s = volumetric bedload transport rate per unit length, C = Chezy roughness, g = acceleration due to gravity, s = specific gravity, D_{50} = median grain size of bed material, and τ^* = Shields parameter, which is implemented as

$$\tau^* = \frac{u^2 + v^2}{C^2(s-1)D_{50}}$$

where u = flow velocity in the streamwise direction and v = flow velocity in the crosswise direction. They state that their implementation of the equation is applicable to sand-bed channels where the suspended sediment load is a substantial portion of the sediment fluxes (Vasquez and Kwan, 2009). Around 99% of the sediment load in the San Antonio River is carried in

suspension.

Sensitivity analysis indicated that the transversal slope factor had no major impact on sediment fluxes when the values varied by ± 0.25 from the default value. Evidence of ripples, dunes, and bedload sheets in the San Antonio River required an adjustment to the sediment transport upwinding factor so that local sediment fluxes explicitly take into account sediment input from upstream grid cells. Increasing the value from the default of 0.25 to 0.9 lowered the sediment load by 82% in the test run. A site specific value for the minimum flow depth needed for sediment transport was set by conducting a sediment entrainment assessment using Shields parameter and flow variables derived from the streamflow rating data of the USGS gauge. Sediment properties were based on the sediment size information derived from field samples. Of the four options for setting boundary conditions of the bed elevation, only the Free option allows for bed adjustment; all others involve fixed elevations at the location of inflow, outflow, or both. The sediment supply entering the study reach can be set to a fixed specific volumetric transport rate but was not activated in this initial modeling given that hydrographs were being modeled. An alternative would be to use an average transport rate for each hydrograph as the upstream sediment supply. Finally, one test run was conducted with the secondary flow correction and associated inertial adaptation length activated but there was very little change in the total sediment flux and patterns of bed adjustment, which may be related to the variability in the radius curvature along the study reach that cannot be captured by a single parameter value.

4.3.4 Model run conditions

For all simulations, the run duration matched the length of the inflow hydrograph because of the relatively short study reach. Using a time step of 10 s and a maximum number of iterations of 9, the equations were solved under fully implicit conditions (i.e., $\text{implicitness} = 1$ under Run morphology) to a solution tolerance of 0.01. Fully implicit computations are recommended when flood hydrographs are being modeled (Steffler and Blackburn, 2002). The solution tolerance of 0.01 is recommended based on a limited number of tests (Steffler and Blackburn, 2002). In this study, sensitivity analysis indicated that the 0.01 tolerance provided a much better match between inflow and outflow hydrographs than a tolerance of 0.1. However, a smaller solution tolerance of 0.005 did not significantly improve the hydrograph correspondence beyond that achieved with the 0.01 tolerance and did not eliminate flow instabilities evident in the outflow hydrograph in the test run. A maximum of 9 iterations is the default value and based on an analysis of model runs is sufficiently large in general. Less than 1% of the iterations required 9 iterations for each flood hydrograph.

4.3.5 Output of results

R2DM allows three main types of output for a given simulation in addition to a computational log from which the outflow hydrograph can be derived.

1) .cdg files at a selected output rate. These individual files can be loaded into R2DM after the simulation to visually evaluate a limited number of variables. Not all variables listed in the software are currently active in R2DM.

2) Video capture of the visible screen display at a selected output rate. Before the beginning of a simulation, the desired variable for the screen display is selected. This mapped variable is then stored in an .avi file that can be played for a visual inspection of how the variable changes over the simulation.

3) .csv output of selected nodes at a selected output rate. Variables that can be selected when using the Engelund-Hansen transport equation include the specific bedload transport rate, roughness, flow depth, and bed elevation.

Given the absence of field data to validate the entire bed area at the resolution of the computational mesh, an output grid was created by positioning 23 channel cross sections throughout the reach (Figure 4). These cross sections cover different areas of the bed morphology and include the three cross sections surveyed for HEC-RAS modeling (i.e., 6, 14, and 23). The spacing is approximately 140 m, with some adjustment to capture different components of the bed morphology (e.g., deepest part of pools).

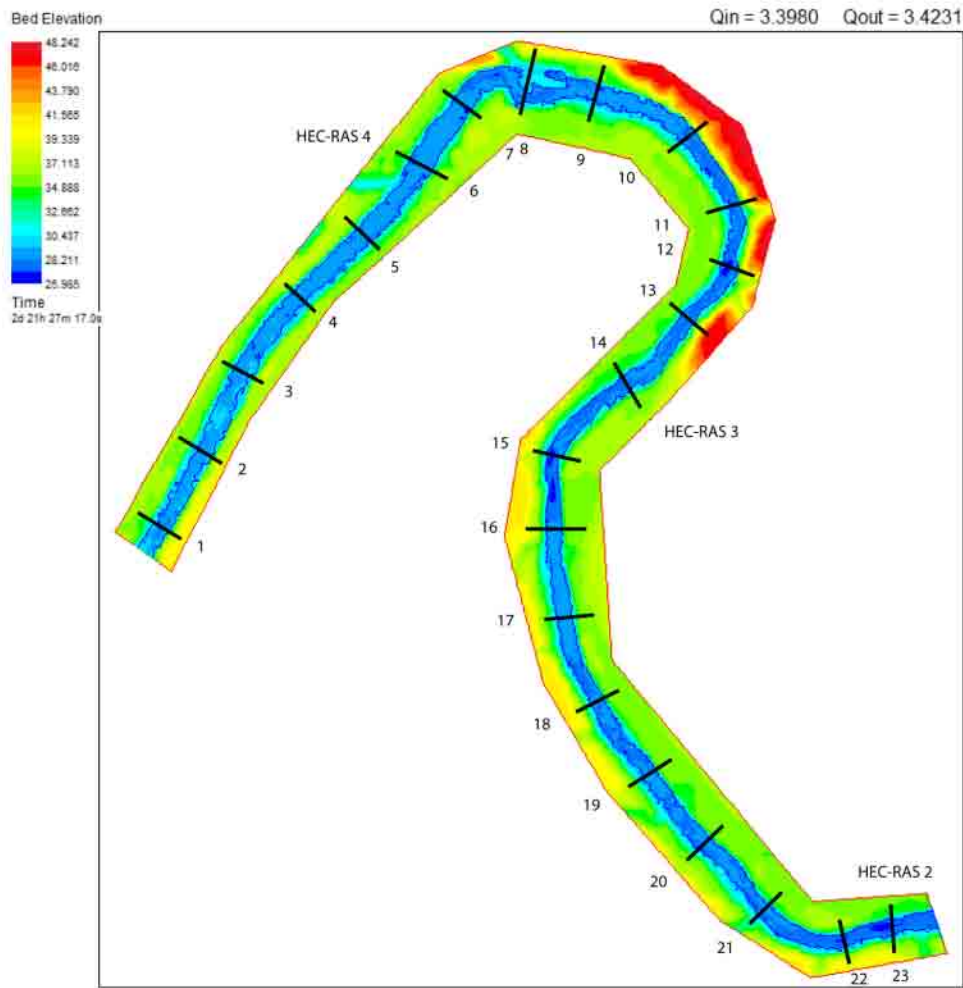


Figure 4. Initial bed morphology of the study reach and the positions of the 23 cross sections used in the analysis of model results

4.3.6 Target flood discharges

The Texas Instream Flow Program focuses on four categories of flows, subsistence, baseflow, pulse, and overbank. In this study modeling was restricted to flood events within channel capacity. Previous work in the study reach gives bankfull discharges of $166 \text{ m}^3\text{s}^{-1}$ ($5863 \text{ ft}^3\text{s}^{-1}$), $210 \text{ m}^3\text{s}^{-1}$ ($7415 \text{ ft}^3\text{s}^{-1}$), and $173 \text{ m}^3\text{s}^{-1}$ ($6114 \text{ ft}^3\text{s}^{-1}$) for HEC-RAS cross sections 4, 3, and 2, respectively (Haschenburger and Curran, 2012). A limit of $156 \text{ m}^3\text{s}^{-1}$ ($5500 \text{ ft}^3\text{s}^{-1}$) was used to ensure the near bankfull discharge was contained within the channel over the entire length of the study reach given the variability in bank height along the river. Subsistence flows were defined as between $1.7 \text{ m}^3\text{s}^{-1}$ ($60 \text{ ft}^3\text{s}^{-1}$) and $2.3 \text{ m}^3\text{s}^{-1}$ ($80 \text{ ft}^3\text{s}^{-1}$), guided by the Lower San Antonio River (LSAR) interim report, but no simulations were completed for this flow category given the very low transport rates expected.

Modeled flood conditions include two floods within conditions of baseflow discharge and three floods that can be considered pulses (Table 6). For the former, baseflow was considered between $2.8 \text{ m}^3\text{s}^{-1}$ ($100 \text{ ft}^3\text{s}^{-1}$) and $4.5 \text{ m}^3\text{s}^{-1}$ ($160 \text{ ft}^3\text{s}^{-1}$) based on the LSAR interim report and a flow duration analysis of the entire streamflow record, respectively. Pulses were selected to cover a range of discharge magnitudes. The associated range in exceedence probability based on mean daily flow is from 51% to 6%.

Table 6. Modeled flood events

Flow	Discharge peak, m^3s^{-1}	Discharge peak, ft^3s^{-1}	Exceedence probability, % ¹
Baseflow 1	2.9	102	0.94
Baseflow 2	4.1	145	0.87
Pulse 1	9.8	346	0.51
Pulse 2	27.5	971	0.16
Pulse 3	64.6	2281	0.055

¹ Based on flow duration of entire flow record of mean daily discharge

Appropriate hydrographs for the target discharges were extracted from the 15 minute streamflow record at the Goliad gauge, concentrating on the most recent portion of the record (Figure 5). Not all hydrographs started from baseflow conditions. The beginning and end of the flood events were truncated or extended to match the nearest available steady flow model (Table 3). When an extension was needed, a discharge-stage relation was used to add estimated stage values. Additionally, each hydrograph was modified to begin with 2.5 hours of a constant flow rate that matched the steady flow model. The minor tributary that enters the reach in the upper section was assumed to have no significant impact on discharge-stage relations.

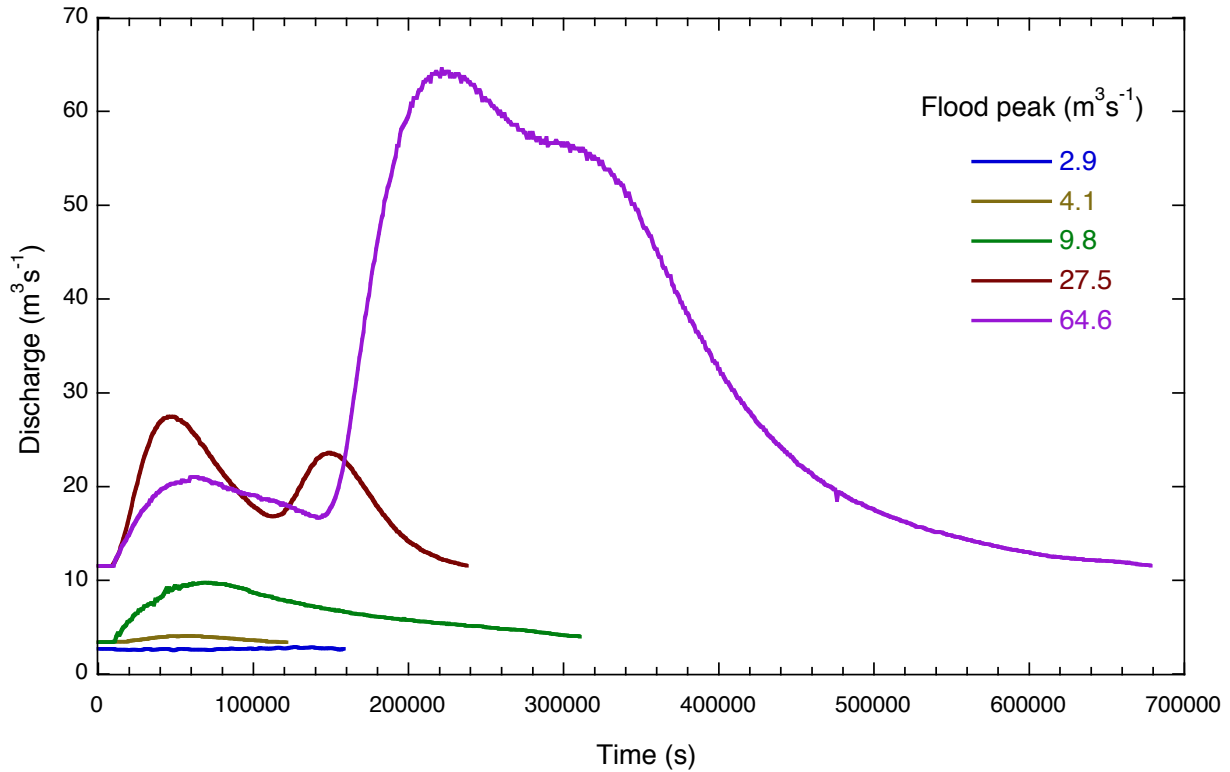


Figure 5. Flood hydrographs for target peak discharges

5 Modeling Results

Analysis of simulation results for the five target hydrographs considers flow characteristics, total bedload flux, and net bed change at the 23 channel cross sections. In the presentation of results, cross sections 1, 2, 22, and 23 are shown in figures for completeness but are not considered in describing numerical ranges and mean values because they are close to the limits of the study reach and most likely influenced by boundary effects.

5.1 Flood peak $2.9 \text{ m}^3 \text{ s}^{-1}$

5.1.1 Flow characteristics

The modeled outflow hydrograph matches the $2.9 \text{ m}^3 \text{ s}^{-1}$ inflow hydrograph reasonably well, except for the initial instability and overprediction during the first portion of the event (Figure 6). Patterns of bed shear stress follow elements of the bed morphology (Figure 7). For example, the deeper pool areas experience higher shear stresses in general.

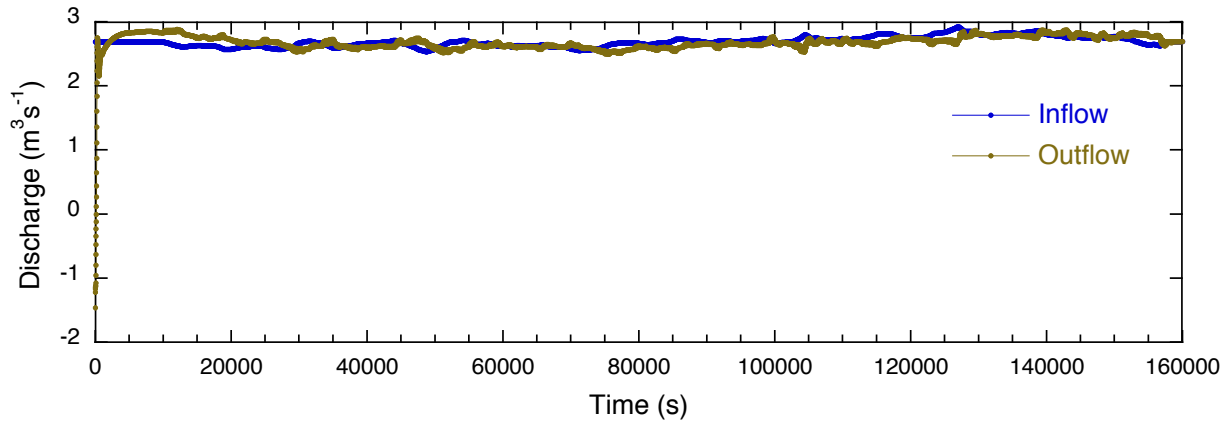


Figure 6. Empirical inflow and modeled outflow hydrographs for the $2.9 \text{ m}^3\text{s}^{-1}$ flood event

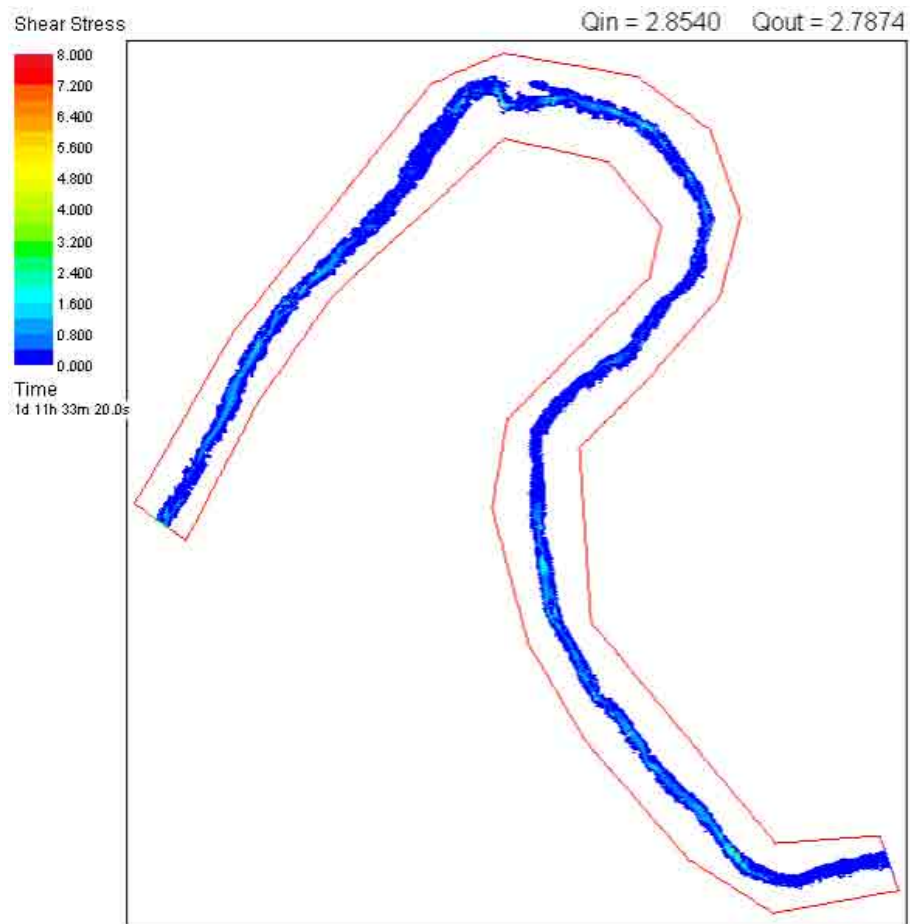


Figure 7. Bed shear stresses near the peak discharge of $2.9 \text{ m}^3\text{s}^{-1}$

5.1.2 Sediment fluxes

The predicted total bedload over the entire event ranges from 46 to 78,455 kg for the 19 cross sections (Figure 8) with a mean flux of $11,387 \pm 4,599 \text{ kg}$. The model overpredicts the bedload

flux compared to that estimated from the bedload rating curve, which equals 1,720 kg.

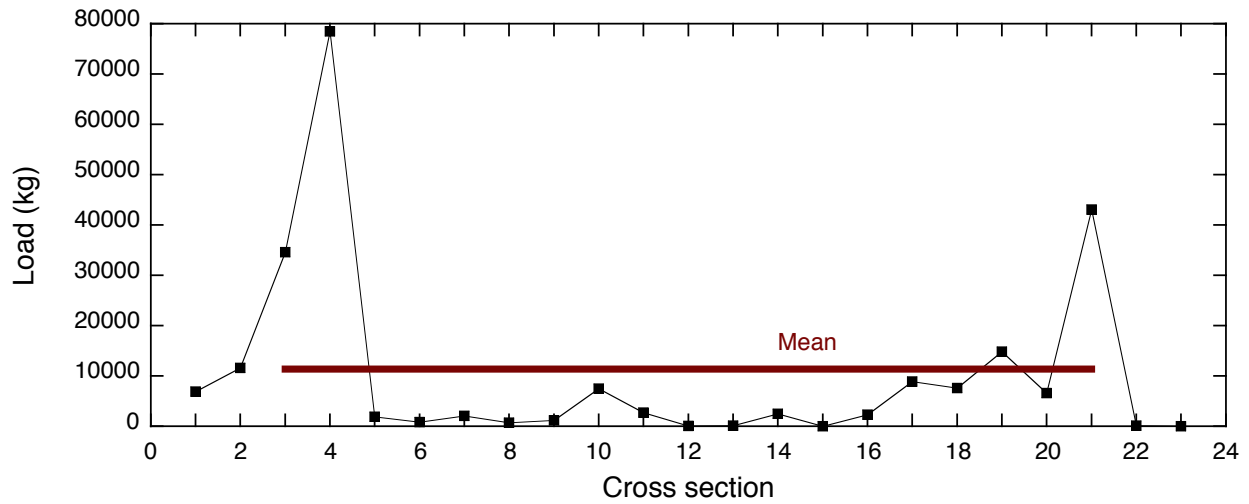


Figure 8. Sediment load by cross section for the $2.9 \text{ m}^3\text{s}^{-1}$ flood event

5.1.3 Net change in the streambed

The net change experienced at the 19 cross sections as a result of the flood ranges from a net erosion of 2.0 m^2 to a net deposition of 0.88 m^2 (Figure 9). Over the reach, the model predicts a net degradation of 1.2 m^2 or a mean depth of net scour of 0.030 m .

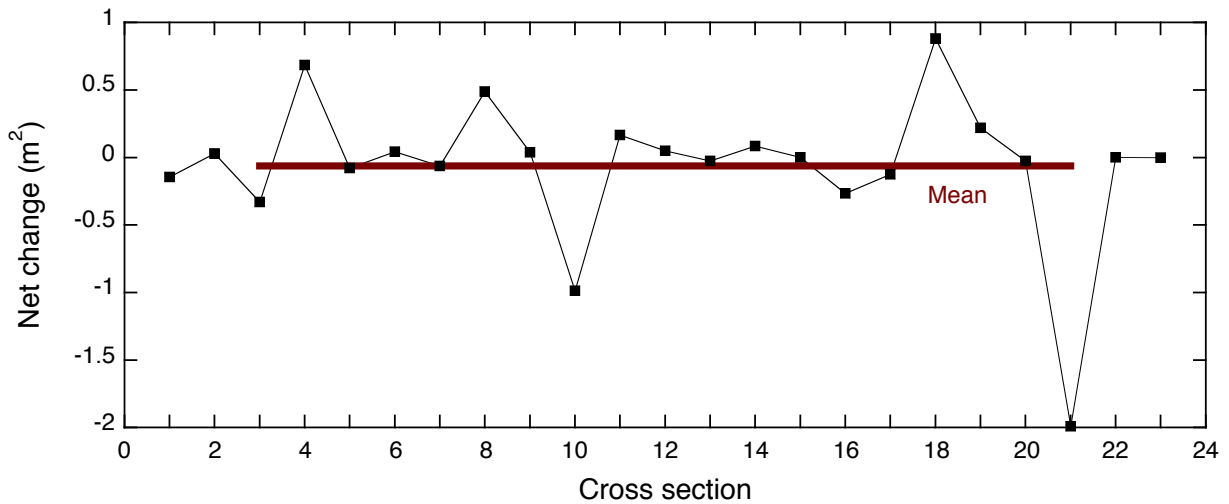


Figure 9. Net change by cross section for the $2.9 \text{ m}^3\text{s}^{-1}$ flood event. Positive and negative numbers indicate net deposition and erosion, respectively.

5.2 Flood peak $4.1 \text{ m}^3\text{s}^{-1}$

5.2.1 Flow characteristics

The modeled outflow hydrograph follows the general trend of the $4.1 \text{ m}^3\text{s}^{-1}$ inflow hydrograph

but periodic instabilities occur over most of the event (Figure 10). However, except for the initial portion of the hydrograph, these discharge fluctuations are not that large. Patterns of bed shear stress show a slight expansion of higher bed stresses compared to the smaller $2.9 \text{ m}^3\text{s}^{-1}$ event as expected (Figure 11).

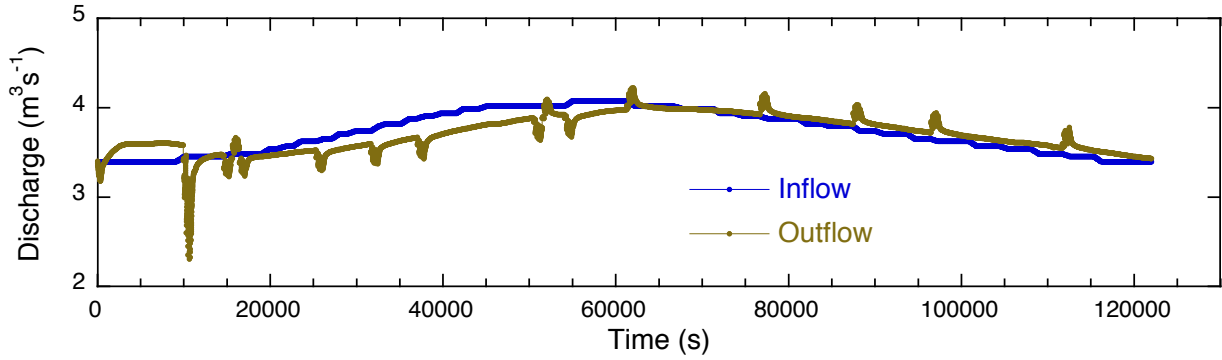


Figure 10. Empirical inflow and modeled outflow hydrographs for the $4.1 \text{ m}^3\text{s}^{-1}$ flood event

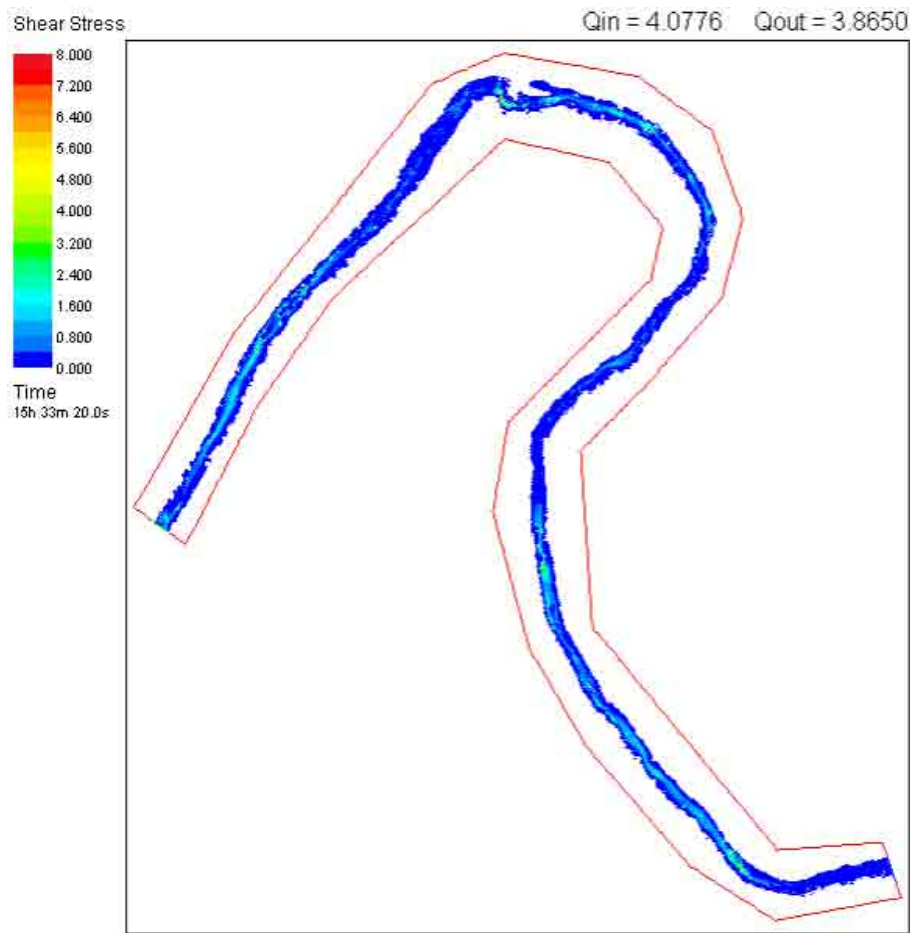


Figure 11. Bed shear stresses near the peak discharge of $4.1 \text{ m}^3\text{s}^{-1}$

5.2.2 Sediment fluxes

The predicted total load over the event ranges from 126 to 103,902 kg for the 19 cross sections (Figure 12) with a mean flux of $16,940 \pm 6,065$ kg. The model overpredicts the total bedload flux when compared to the 2,638 kg estimated from the bedload rating curve.

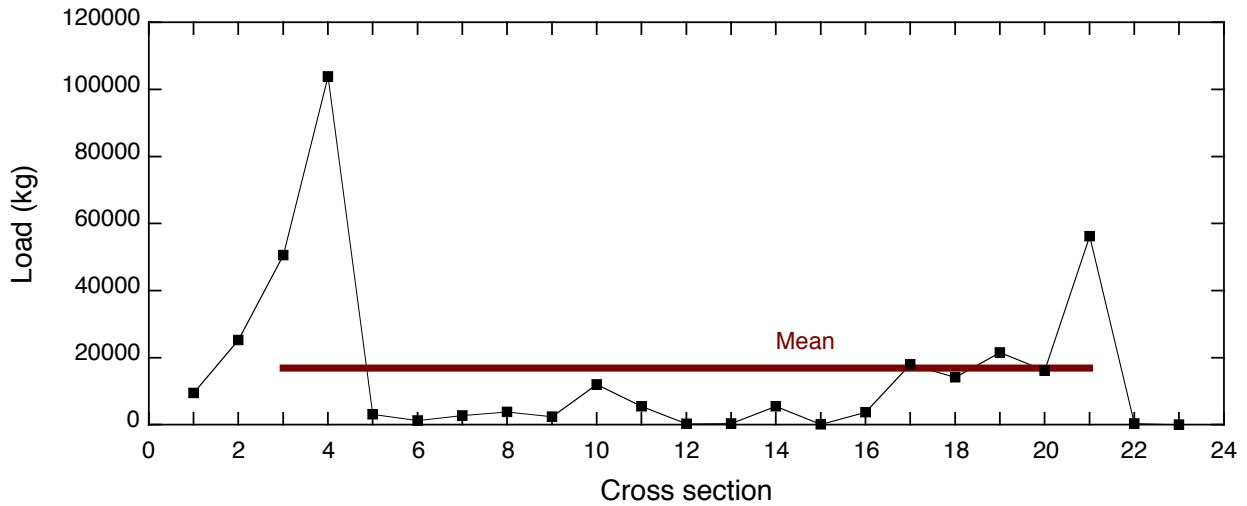


Figure 12. Sediment load by cross section for the $4.1 \text{ m}^3\text{s}^{-1}$ flood event

5.2.3 Change in bed morphology

The net change experienced at the 19 cross sections as a result of the flood ranges from a net erosion of 2.5 m^2 to a net deposition of 1.4 m^2 (Figure 13). Over the reach, the model predicts a net degradation of 1.2 m^2 or a mean depth of net scour of 0.029 m .

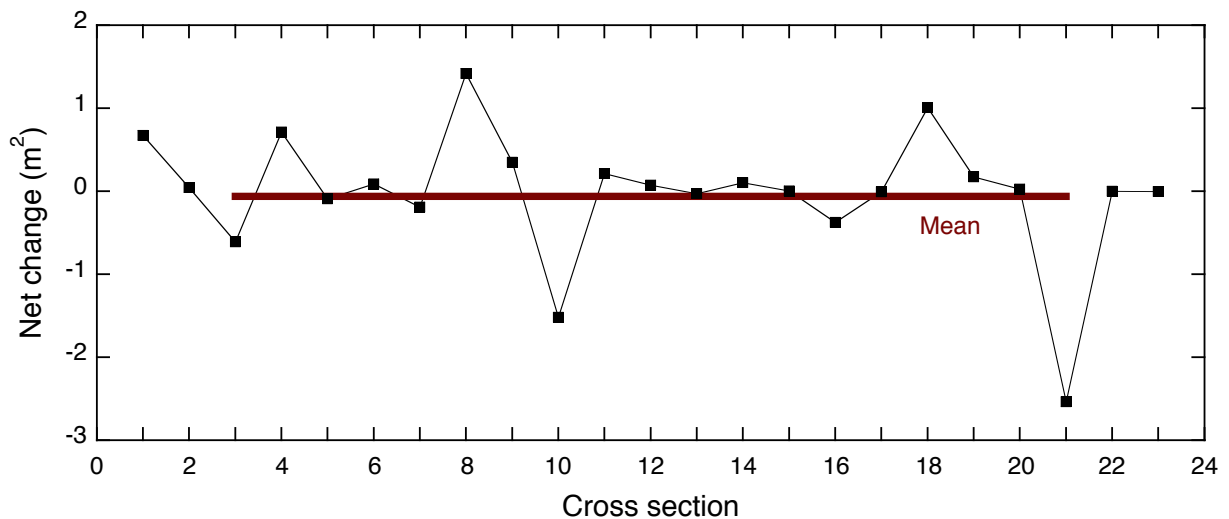


Figure 13. Net change by cross section for the $4.1 \text{ m}^3\text{s}^{-1}$ flood event. Positive and negative numbers indicate net deposition and erosion, respectively.

5.3 Flood peak $9.8 \text{ m}^3 \text{ s}^{-1}$

5.3.1 Flow characteristics

The modeled outflow hydrograph follows the general trend of the $9.8 \text{ m}^3 \text{ s}^{-1}$ inflow hydrograph but exhibits periodic instabilities that are most pronounced on the rising limb (Figure 14). Bed shear stresses increase to higher values compared to the $4.1 \text{ m}^3 \text{ s}^{-1}$ event as expected (Figure 15).

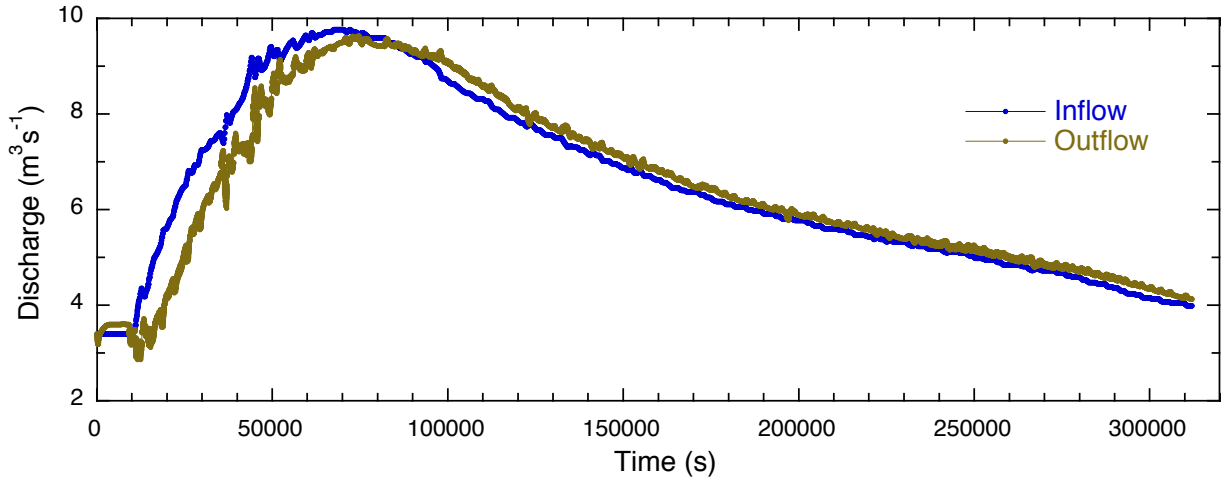


Figure 14. Empirical inflow and modeled outflow hydrographs for the $9.8 \text{ m}^3 \text{ s}^{-1}$ flood event

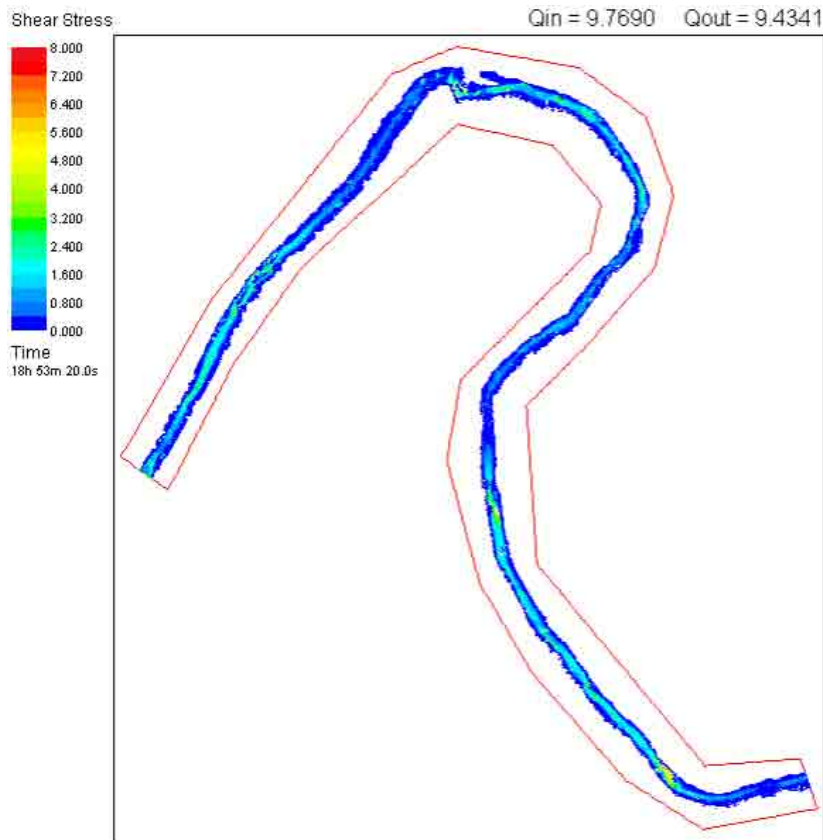


Figure 15. Bed shear stresses near the peak discharge of $9.8 \text{ m}^3 \text{ s}^{-1}$

5.3.2 Sediment fluxes

The predicted total load over the event ranges from 2,089 to 250,033 kg for the 19 cross sections (Figure 16) with a mean flux of $67,564 \pm 16,683$ kg. The model overpredicts the total bedload flux when compared to the 11,311 kg estimated from the bedload rating curve.

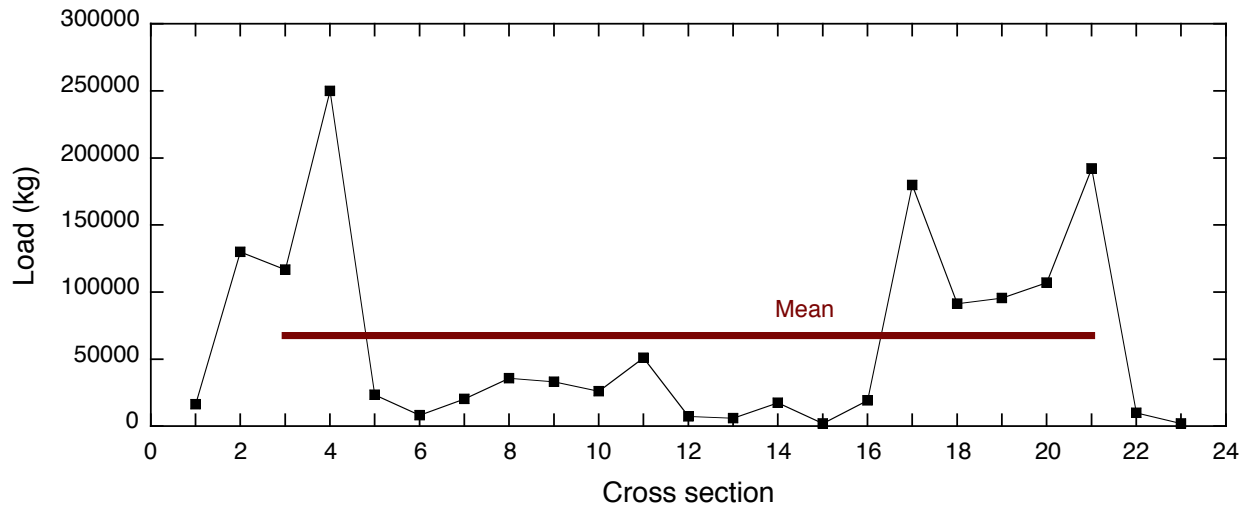


Figure 16. Sediment load by cross section for the $9.8 \text{ m}^3\text{s}^{-1}$ flood event

5.3.3 Change in bed morphology

The net change experienced at the 19 cross sections as a result of the flood ranges from a net erosion of 8.6 m^2 to a net deposition of 7.3 m^2 (Figure 17). Over the reach, the model predicts a net degradation of 2.8 m^2 or a mean depth of net scour of 0.070 m .

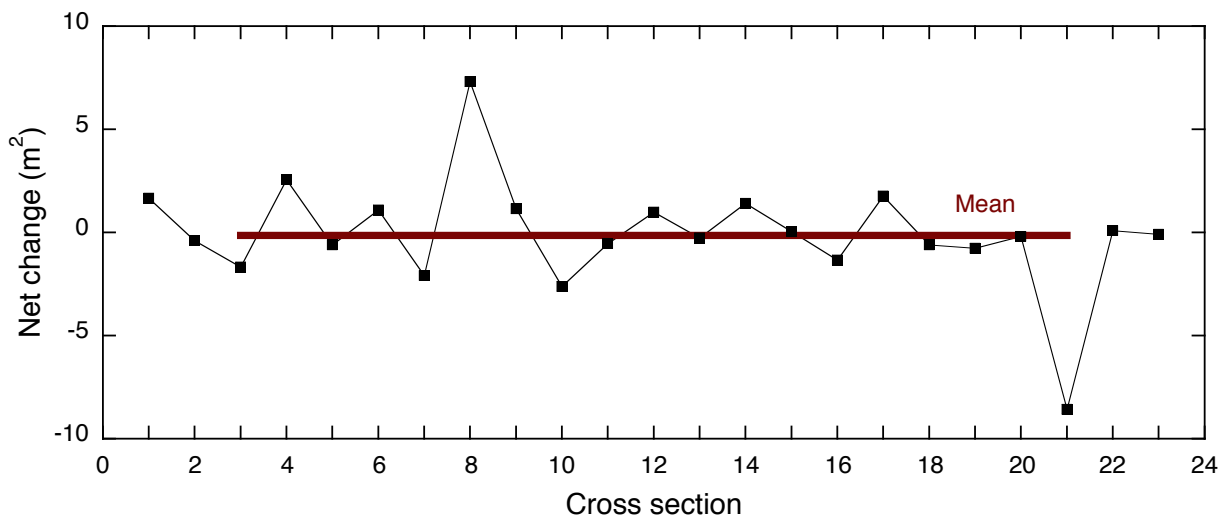


Figure 17. Net change by cross section for the $9.8 \text{ m}^3\text{s}^{-1}$ flood event. Positive and negative numbers indicate net deposition and erosion, respectively.

5.4 Flood peak $27.5 \text{ m}^3\text{s}^{-1}$

5.4.1 Flow characteristics

The modeled outflow hydrograph matches the $27.5 \text{ m}^3\text{s}^{-1}$ inflow hydrograph well except initially (Figure 18). Higher bed shear stresses increase in spatial extent as expected (Figure 19).

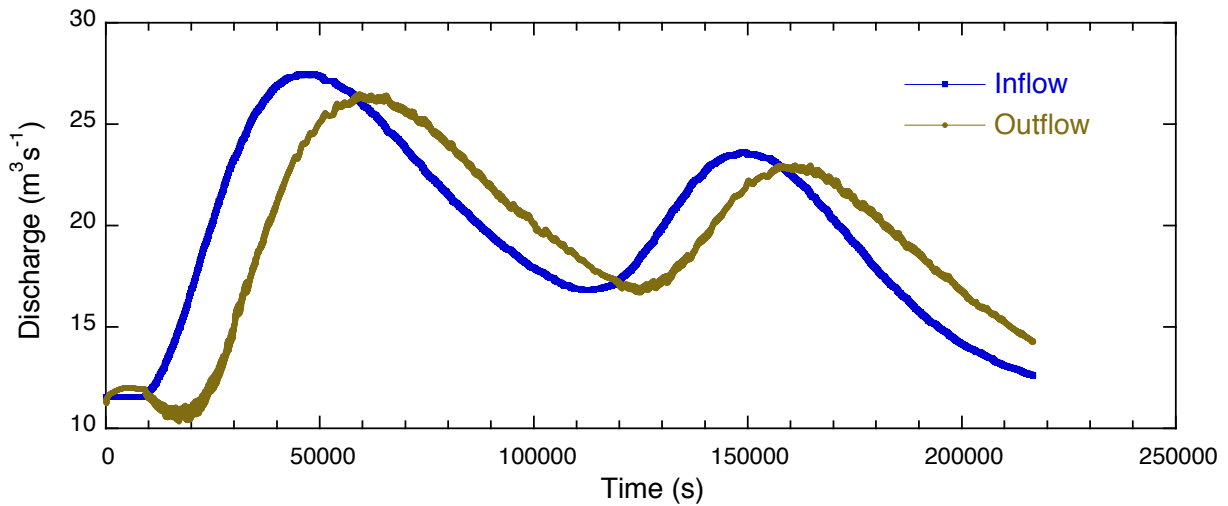


Figure 18. Empirical inflow and modeled outflow hydrographs for the $27.5 \text{ m}^3\text{s}^{-1}$ flood event

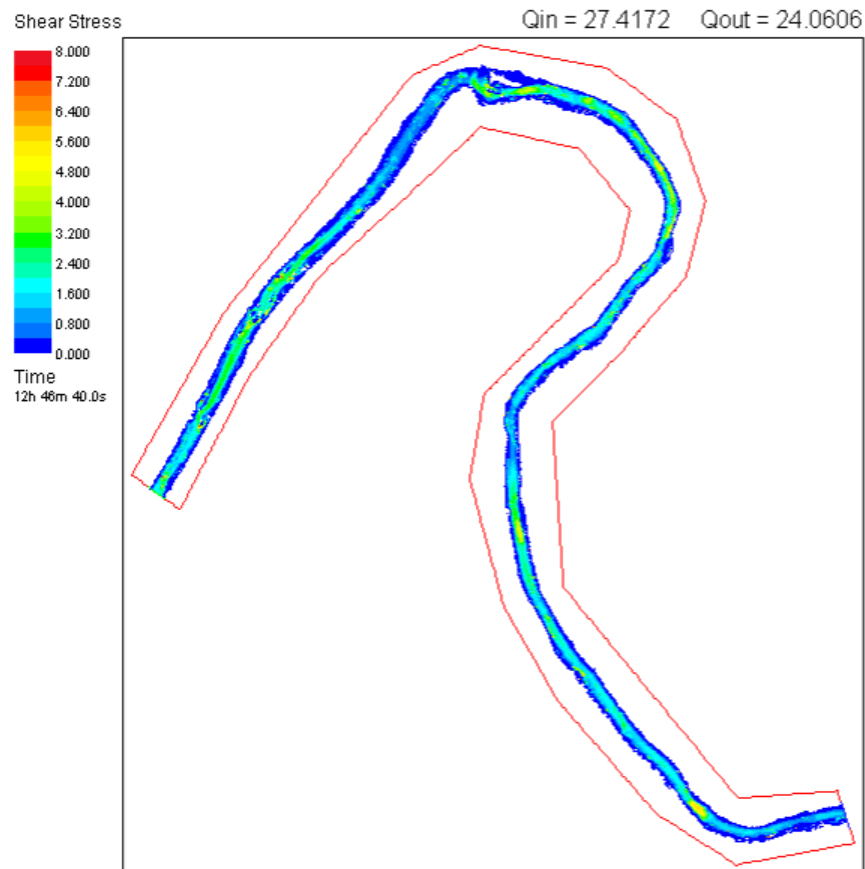


Figure 19. Bed shear stresses near the peak discharge of $27.5 \text{ m}^3\text{s}^{-1}$

5.4.2 Sediment fluxes

The predicted total load over the event ranges from 34,119 to 776,567 kg for the 19 cross sections (Figure 20) with a mean flux of $231,578 \pm 41,336$ kg. The model overpredicts the total bedload flux compared to that estimated from the bedload rating curve, which amounts to 34,114 kg.

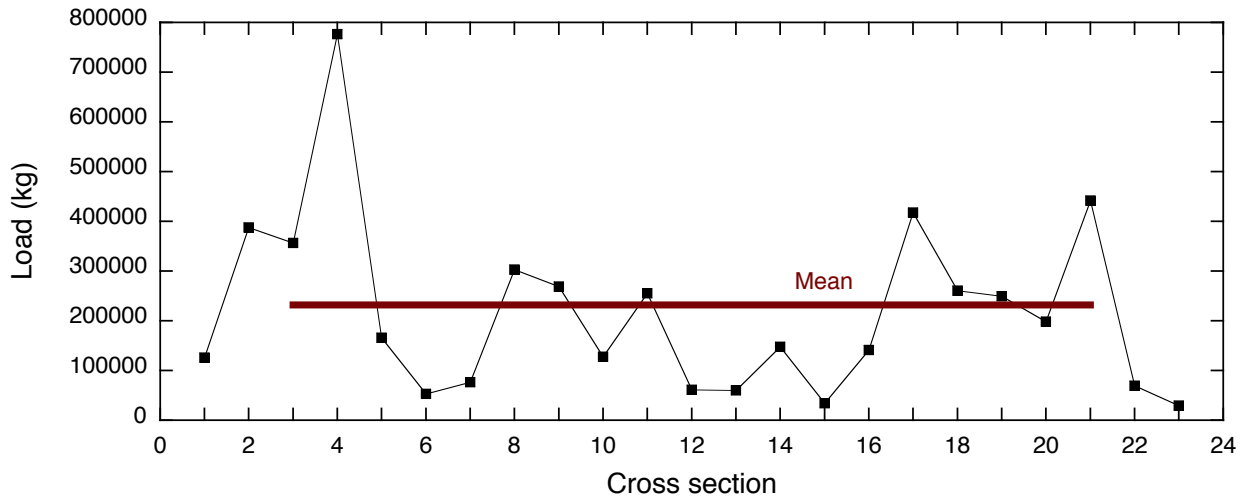


Figure 20. Sediment load by cross section for the $27.5 \text{ m}^3\text{s}^{-1}$ flood event

5.4.3 Change in bed morphology

The net change experienced at the 19 cross sections as a result of the flood ranges from a net erosion of 5.2 m^2 to a net deposition of 14.4 m^2 (Figure 21). Over the reach, the model predicts a net aggradation of 28.65 m^2 or a mean depth of net fill of 0.72 m .

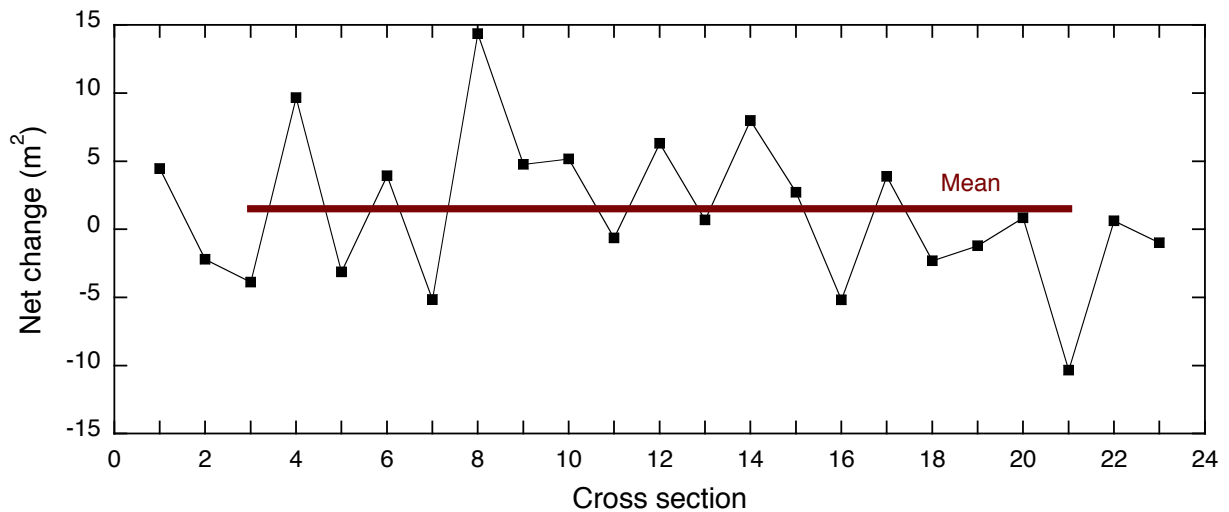


Figure 21. Net change by cross section for the $27.5 \text{ m}^3\text{s}^{-1}$ flood event. Positive and negative numbers indicate net deposition and erosion, respectively.

5.5 Flood peak $64.6 \text{ m}^3\text{s}^{-1}$

5.5.1 Flow characteristics

The modeled outflow hydrograph follows the $64.6 \text{ m}^3\text{s}^{-1}$ inflow hydrograph quite well but there are instabilities initially and near the peak (Figure 22). Bed shear stress increases with a notable shift in high stresses over the channel bar present in the widest area of the reach (Figure 23).

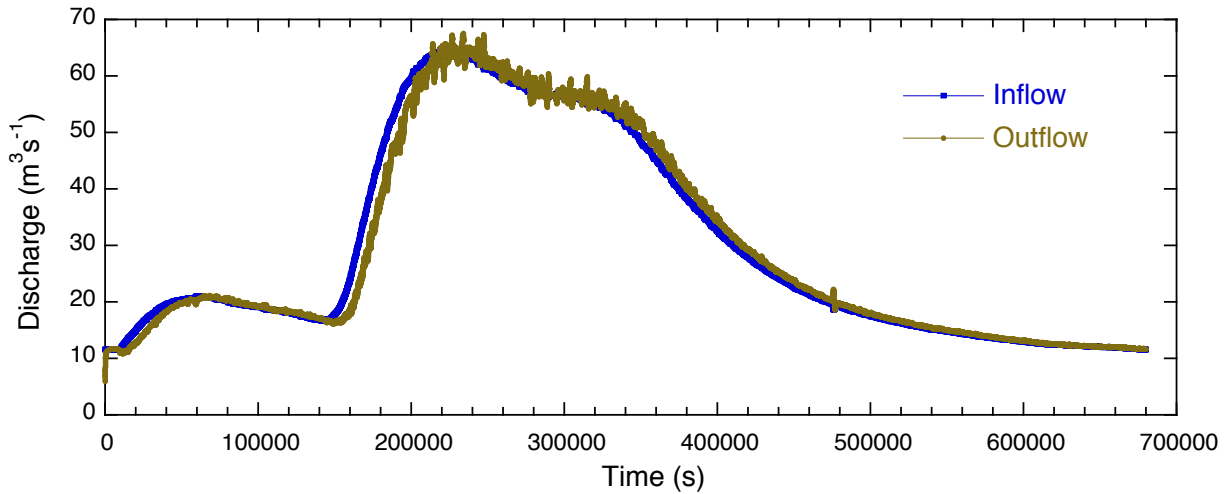


Figure 22. Empirical inflow and modeled outflow hydrographs for the $64.6 \text{ m}^3\text{s}^{-1}$ flood event

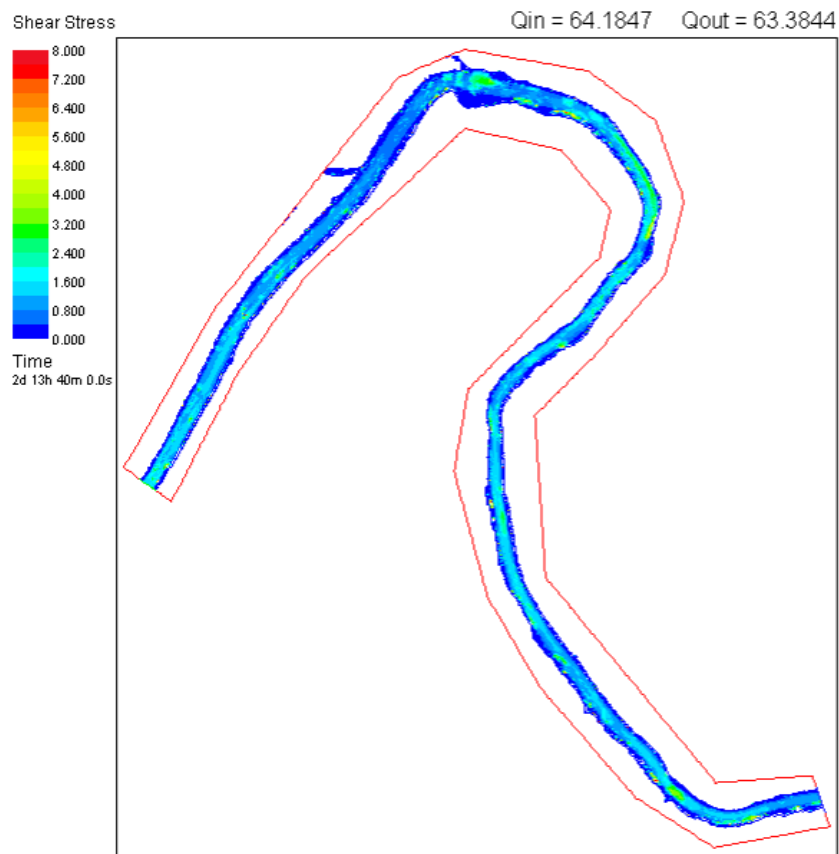


Figure 23. Bed shear stresses near the peak discharge of $64.6 \text{ m}^3\text{s}^{-1}$

5.5.2 Sediment fluxes

The predicted total load over the event ranges from 149,721 to 1,565,414 kg for the 19 cross sections (Figure 24) with a mean flux of $547,017 \pm 79,185$ kg. The model overpredicts the total bedload flux when compared to the 196,951 kg determined from the bedload rating curve.

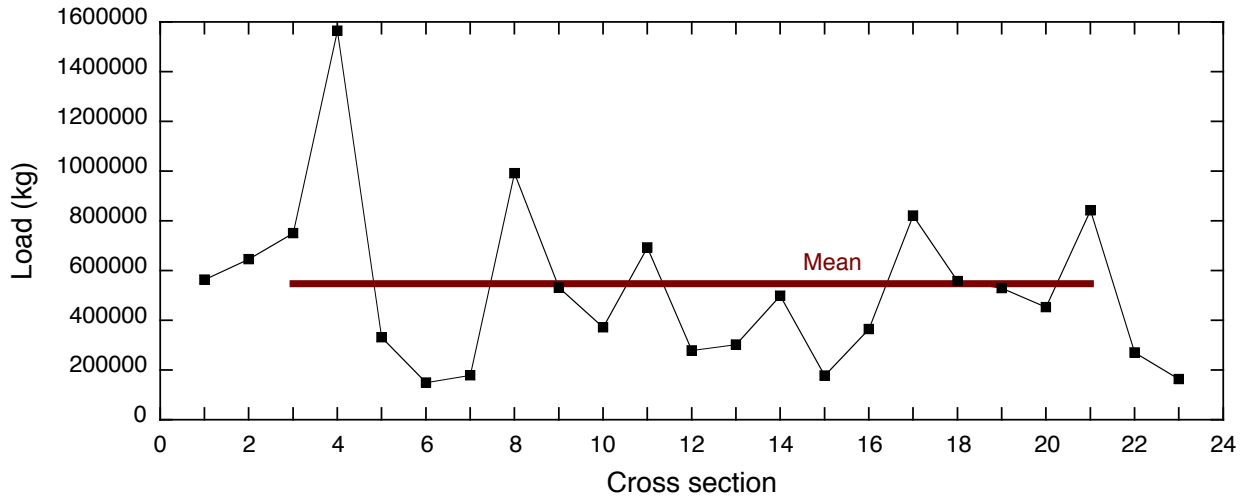


Figure 24. Sediment load by cross section for the $64.6 \text{ m}^3 \text{ s}^{-1}$ flood event

5.5.3 Change in bed morphology

The net change experienced at the 19 cross sections as a result of the flood ranges from a net erosion of 16.4 m^2 to a net deposition of 18.3 m^2 (Figure 25). Over the reach, the model predicts a net aggradation of 31.0 m^2 or a mean depth of net fill of 0.77 m .

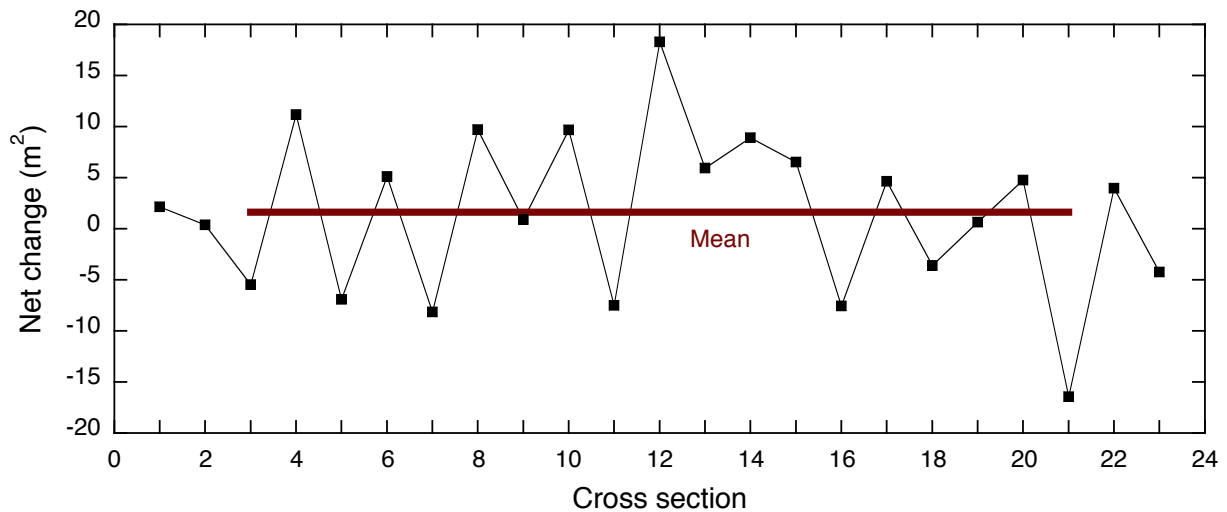


Figure 25. Net change by cross section for the $64.6 \text{ m}^3 \text{ s}^{-1}$ flood event. Positive and negative numbers indicate net deposition and erosion, respectively.

5.6 Summary of model performance

Based on the evaluated flood hydrographs R2DM captures the overall temporal trends of the floods but short duration instabilities exist over most events. The initial instabilities may reflect the transition from a steady flow model to an unsteady flow model, because the flow upwinding parameter changes from the recommended value of 0.5 to 0.25. However, the addition of a 2.5 hour period with a constant flow rate equal to the steady flow model did not eliminate the initial instabilities. In stabilities that subsequently occur are probably associated with the wetting and drying of bed areas as the flow rate changes. In the sensitivity analysis, the magnitude of the instabilities decreased somewhat with a decrease in the groundwater storage parameter (Figure 3), suggesting that the surface-groundwater exchange process plays at least a partial role.

The model predicts spatial variability in bedload fluxes as would be expected, even over short distances (Haschenburger and Church, 1998), but the range in these fluxes appears too large, spanning one to three orders of magnitude. Additionally, although the model predicts total fluxes that generally scale with flow magnitude, the loads are significantly larger than those derived from the bedload rating curve. The overprediction is most likely linked to the sediment transport function, although the Engelund-Hanson equation is the best choice in R2DM based on its development and calibration. Bedload is very difficult to predict accurately due to the uncertainties associated with capturing the essential details of the flow hydraulics and predicting initial sediment motion. Further, the assumption of equilibrium transport generally embedded in transport equation development tends to lead to overprediction because this condition is not typically achieved in natural channels.

In terms of net change in the streambed, only an order of magnitude comparison is possible because of the longer time scale of the available field observation of net bed change (Table 9). The model results are within the general range of these observations, especially considering the possible cumulative effect of the nine flood events captured in the observed estimates of change. Although no net degradation is modeled for the two cross sections, there is evidence of this at other cross sections (Figures 9, 13, 17, 21 and 25). When the maximum range in modeled net change is considered, some cross sections are changing at the order of magnitude determined by field observation.

Table 9. Observed and modeled changes in cross-sectional area¹

Cross section	Observed		Modeled				
	Time period of observed change	Net change, m ²	Net change for individual events, m ²				
			2.9 m ³ s ⁻¹	4.1 m ³ s ⁻¹	9.8 m ³ s ⁻¹	27.5 m ³ s ⁻¹	64.6 m ³ s ⁻¹
6	7/29/09-2/10/10	0.6	0.04	0.09	1	4	5
14	8/8/09-2/10/10	-28	0.08	0.1	1	8	9

¹ Positive numbers indicate net deposition and negative numbers indicate net erosion; cross section 23 (HEC-RAS 2) was not evaluated due to its proximity to the downstream boundary of the study reach

6 Conclusion

The R2DM model for the Goliad reach captures spatial variability in bedload fluxes and bed adjustment that are expected in general but overpredicts the magnitude of fluxes. Future refinement of the model should consider at least five aspects. First, further work is needed to resolve the instabilities in the outflow hydrograph, which probably relate, at least in part, to modeling the wetting and drying of the streambed as discharge changes. Such resolution will likely improve the accuracy of modeling the areal extent and timing of flow expansion and contraction over the streambed during floods and associated sediment fluxes and bed adjustments. Second, the most appropriate sediment transport equation available in R2DM was used, which suggests that alternative equations would be worth pursuing. It may be possible to work with the R2DM developers to incorporate alternative equations for the conditions of the San Antonio River. Third, model results are based on one computational mesh. Further work should use different meshes to explore how sensitive results are to a given mesh. Additionally, in executing the simulations, computational times are long so that modeling a longer section of the flood record will be very time intensive. However, increasing cell size and trimming the mesh file to the floodplain-bank interface would help to decrease the duration of simulations by reducing the computational mesh. Fourth, collection of a comprehensive set of field observations during individual flood events would help to improve the calibration of the model for unsteady flow. Fifth, this initial modeling used discrete flood hydrographs with the same initial bed morphology. This is a simplification that does not allow for bed adjustments achieved over a series of flood events or a bed morphology for a given flood in the sequence that is determined by the preceding events. Once the first four aspects are resolved or improved, further modeling should explore the influence of a flood series on streambed adjustment. Finally, it should be noted that the depiction of bed adjustment was limited to discrete cross sections. Once bed adjustments are quantified by repeat bathymetry, results from the entire computation mesh can be evaluated. This increased spatial resolution will necessitate a more sophisticated strategy for handling output files because the .csv output files quickly exceed the size limit of Excel files based on the array arrangement of output variables, the number of computational nodes, and the number of time increments.

7 References cited

- Engelund, F. and E. Hansen, 1967, A monograph on sediment transport in alluvial streams. Teknisk Forlag, 62 pp.
- Haschenburger, J.K. and J. Curran, 2012, Sediment transport modeling of reach scale geomorphic processes. Final report for TWDB contract number 0904830899, 38 pp.
- Haschenburger, J.K. and M. Church, 1998, Bed material transport estimated from the virtual velocity of sediment. *Earth Surface Processes and Landforms*, 23, 791-808.
- Hicks, F.E. and P.M. Steffler, 1992, Characteristic dissipative Galerkin scheme for open-channel flow. *Journal of Hydraulic Engineering*, 118, 337-352.
- Kassem, A.A. and M.H. Chaudhry, 1998, Comparison of coupled and semi-coupled numerical

- models for alluvial channels. *Journal of Hydraulic Engineering*, 124, 794-802.
- Komura, S., 1961, Bulk properties of river bed sediments, its applications to sediment hydraulics, *Proc. 11th Japan National Congress for Applied Mechanics*, pp. 227-231.
- Meyer-Peter, E. and R. Müller, 1948, Formulas for bed-load transport, *Proceedings 2nd Meeting International Association for Hydraulic Research, Stockholm*, pp. 39-64.
- Steffler, P. and J. Blackburn, 2002, *River2D: Two-dimensional depth averaged model of river hydrodynamics and fish habitat. Introduction to depth averaged modeling and user's manual*, 119 pp.
- van Rijn, L.C., 1984, Sediment transport, part I: bed load transport. *Journal of Hydraulic Engineering*, 110, 1431-1456.
- Vasquez, J. and S. Kwan, 2009, *River2D-Morphology user manual for version 5.0*, 34 pp.
- Wilcock, P.R. and J.C. Crowe, 2003, Surface-based transport model for mixed-size sediment. *Journal of Hydraulic Engineering*, 129, 120-128.